Four-State Equilibrium Unfolding of an scFv Antibody Fragment†

Idolka Pedroso, María P. Irún, Claudia Machicado, and Javier Sancho*

Departamento de Bioquímica y Biología Molecular y Celular, Facultad de Ciencias, Universidad de Zaragoza, 50009 Zaragoza, Spain

Received February 27, 2002; Revised Manuscript Received June 5, 2002

ABSTRACT: The conformational stability of a single-chain Fv antibody fragment against a hepatitis B surface antigen (anti-HBsAg scFv) has been studied by urea and temperature denaturation followed by fluorescence and circular dichroism. At neutral pH and low protein concentration, it is a well-folded monomer, and its urea and thermal denaturations are reversible. The noncoincidence of the fluorescence and circular dichroism transitions indicates the accumulation in the urea denaturation of an intermediate (I_1) not previously described in scFv molecules. In addition, at higher urea concentrations, a red-shift in the fluorescence emission maximum reveals an additional intermediate (I_2), already reported in the denaturation of other scFvs. The urea equilibrium unfolding of the anti-HBsAg scFv is thus four-state. A similar four-state behavior is observed in the thermal unfolding although the intermediates involved are not identical to those found in the urea denaturation. Global analysis of the thermal unfolding data suggests that the first intermediate displays substantial secondary structure and some well-defined tertiary interactions while the second one lacks well-defined tertiary interactions but is compact and unfolds at higher temperature in a noncooperative fashion. Global analysis of the urea unfolding data (together with the modeled structure of the scFv) provides insights into the conformation of the chemical denaturation intermediates and allows calculation of the N−I_1, I_1−I_2, and I_2−D free energy differences. Interestingly, although the N−D free energy difference is very large, the N−I_1 one, representing the 'relevant' conformational stability of the scFv, is small.

Single-chain Fv fragments (scFvs)[1] constitute interesting alternatives to the use of whole antibody molecules (*1*−*3*). A major problem in the use of scFvs is their tendency to aggregate after purification, which has been related to several factors including the presence or absence of a disulfide bridge in the V_H domain (*4*); exposed hydrophobic patches at the variable/constant domains interface (*5*); and ionic strength, pH, and linker length (*6*). scFv aggregation should be alleviated by a deeper understanding of the noncovalent interactions that stabilize the folded and intermediate conformations of proteins, so that undesirable states could be prevented or destabilized (*7, 8*). On the other hand, a detailed description of the intrinsic conformational complexity of the scFv molecule, in as wide a range of conditions as possible, could help to guide scFv purification, storage, and usage.

Although scFv intermediates with secondary structure have been observed, simple two-state models have often been used to fit thermodynamic data from solvent denaturation studies (*9, 10*). More recently, the equilibrium unfolding of scFv molecules has been described as being three-state (*4, 11, 12*), but a global analysis of the unfolding equilibrium combining data obtained using different spectroscopic techniques is still lacking. There is much current interest in determining the extent to which related proteins share stability and folding features (*13*). Toward that end, exploring the complexity of the scFv folding equilibrium will open the possibility to investigate whether this increasingly useful protein family displays a common equilibrium pattern.

In this paper, we investigate, using fluorescence and circular dichroism, the equilibrium unfolding of an scFv derived from CB-HEP1 (*14*), a mouse antibody used for affinity purification of a recombinant hepatitis B surface antigen virus [r-HBsAg (*15*)]. The scFv contains 254 residues (including 6 Trp, 14 Tyr, and 10 Pro) and consists of 2 beta sandwiches, corresponding to the V_H and V_L domains from the parent antibody. The packing of the two domains reduces the solvent accessibility of some of the Trp residues. In solution conditions where the scFv is monomeric and experiences reversible denaturation, we observe the accumulation of two sequential equilibrium intermediates, in both thermal and urea unfolding. From global analyses of the thermal and of the urea unfolding data obtained using different spectroscopic techniques at different pH values, we determine the temperature, urea concentration, and pH intervals where the native conformation is dominant, the free energy differences of the three urea denaturation equilibria, and some properties of the intermediates. The possible

† We acknowledge financial support from Grants 2FD1997-0758 (FEDER+DGES, Spain), PB97-1027 (DGES, Spain), BMC2001-2522 (MCYT, Spain), and P15/97 (CONSI+D, DGA, Spain). M.P.I. was supported by an FPU fellowship. I.P. was partly supported and C.M. was supported by AECI (Spain) fellowships.

* Correspondence should be addressed to this author at the Departamento de Bioquímica y Biología Molecular y Celular, Facultad de Ciencias, Universidad de Zaragoza, 50009 Zaragoza, Spain. Phone: (34) 976761286. FAX: (34) 976762123. E-mail: jsancho@posta.unizar.es.

[1] Abbreviations: scFv, single-chain Fv antibody fragment; V_H, variable domain of the heavy chain; V_L, variable domain of the ligh chain; HbsAg, hepatitis B surface antigen virus; CD, circular dichroism; CDR, complementarity determining region.

10.1021/bi025742e CCC: $22.00
Published on Web 07/09/2002

structures of these intermediates and their relationship with the one described by Wörn and Plückthun (*16*) for other scFv molecules are discussed.

MATERIALS AND METHODS

Purification and Quantitation of scFv. The anti-HBsAg scFv fragment was expressed and purified as described (*17*). Briefly, the V_H-linker-V_L scFv gene was cloned into pPACIB.1, a vector designed for antibody fragment expression in *E. coli* under the control of a tryptophan promoter, a T4 phage termination signal, and an ompA signal peptide for periplasm export (*18*). The exported scFv molecule contains a six-histidine N-terminal tail and forms inclusion bodies. After cell disruption, the scFv is extracted from the insoluble cell material with urea, purified by immobilized metal ion affinity chromatography, renatured by dialysis to recover its anti-HBsAg activity, concentrated, and further purified by molecular exclusion chromatography.

The concentration of the scFv was determined from its absorbance at 280 nm (*19*) using an extinction coefficient of 50 654 M^{-1} cm^{-1}.

Absorbance, Fluorescence, and Circular Dichroism. Absorbance spectra were recorded at 25.0 ± 0.1 °C in a Kontron Uvikon 860 spectrophotometer. Fluorescence emission spectra (excitation at 280 nm) were acquired at 25.0 ± 0.1 °C in a Kontron SMF 25 or in an Aminco Bowman Series 2 fluorometer using a 1 μM protein concentration in 2 mM boric acid, 2 mM sodium phosphate, 2 mM sodium citrate, and 25 mM NaCl. Circular dichroism spectra were recorded in a Jasco 710 spectropolarimeter at 25.0 ± 0.1 °C in a 1 cm cuvette, using a 1 μM protein concentration for the far-UV spectra and 10 μM for the near-UV ones. For the recording of unfolding curves, cuvettes of different path lengths and various protein concentrations were used, as stated in the figure legends.

Determination of scFv Molecular Mass and Stokes Radius. The scFv apparent molecular mass was determined by molecular exclusion chromatography using an FPLC system (Pharmacia) with a Superose 12HR 10/30 column equilibrated in 2 mM boric acid, 2 mM sodium phosphate and 2 mM sodium citrate, 100 mM NaCl, at different pH values. The Stokes radius was determined from the apparent molecular mass, using the general equation proposed by Uversky (*20*).

pH Denaturation. The unfolding transition observed by fluorescence at high pH was fitted to eq 1:

$$y = \frac{y_U + y_N 10^{(pH - pK_a)}}{1 + 10^{(pH - pK_a)}} \quad (1)$$

that assumes the transition is associated with the titration of a single ionizable group (*21*). In eq 1, y_U is the fluorescence of the denatured, deprotonated form, and y_N is the fluorescence of the folded, protonated form. The pK_a corresponds to the midpoint of the pH transition.

Three-State Analysis of Urea Denaturation Data. Urea unfolding curves at pH 7.0 were monitored by fluorescence emission (360/320 nm ratio, excitation at 280 nm) and circular dichroism (231 nm). The buffer was 2 mM boric acid, 2 mM sodium phosphate, 2 mM sodium citrate at pH 7. The unfolding curves were protein concentration independent below 4 μM. The data were first fitted to a two-state equilibrium assuming a linear relationship between free energy and urea concentration (*22, 23*), using eq 2:

$$y = \frac{y_N + y_U e^{-(\Delta G_w - mD)/RT}}{1 + e^{-(\Delta G_w - mD)/RT}} \quad (2)$$

where y is the observed signal, y_N the signal of the folded state, y_U the signal of the unfolded state, ΔG_w the standard free energy difference between the folded and unfolded states in the absence of denaturant, D the concentration of denaturant, and m the slope of a linear plot of ΔG versus D.

The optical data were then transformed to apparent unfolded fractions (*24, 25*) using eq 3:

$$F_{app} = \frac{y - y_N}{y_U - y_N} \quad (3)$$

Transformed fluorescence and circular dichroism urea unfolding curves were globally fitted to a three-state model (states A, B, and C) using the following relationship:

$$F_{app} = \frac{Z + K_{BC}}{1 + 1/K_{AB} + K_{BC}} \quad (4)$$

where the equilibrium constants follow eqs 5 and 6:

$$K_{AB} = e^{-\Delta G_{AB}/RT} \quad (5)$$

$$K_{BC} = e^{-\Delta G_{BC}/RT} \quad (6)$$

and the equilibria standard free energies are related to the concentration of denaturant (D) by the following linear relationships:

$$\Delta G_{AB} = \Delta G_{AB,w} - m_{AB} D \quad (7)$$

$$\Delta G_{BC} = \Delta G_{BC,w} - m_{BC} D \quad (8)$$

In eq 4, the Z parameter represents the degree of spectroscopic similarity between the intermediate and denatured states ($Z = 1$ if the intermediate resembles the denatured state and $Z = 0$ if it resembles the native one). In the global analysis, the Z parameter may take different values for the different techniques used to monitor the unfolding (in this case fluorescence and circular dichroism), but the free energy differences and their denaturant concentration dependencies are forced to be the same for all the curves globally analyzed.

Thermal Denaturation. Thermal unfolding was followed by fluorescence emission (320/360 nm ratio, excitation at 280 nm; 1 μM scFv) and circular dichroism (212 nm, 1 μM scFv or 294 nm, 10 μM scFv). The buffer was 2 mM boric acid, 2 mM sodium phosphate, 2 mM sodium citrate, and 25 mM NaCl. For the far-UV CD curves, 1 mM buffering salts were used, and the ionic strength was kept constant with NaCl. The temperature, monitored with a thermocouple immersed in the cuvette, was increased from 25 to 80 °C. The unfolding curves were first analyzed using a two-state equation (eq 9) as described (*26*):

$$y = \frac{y_N + y_U e^{-(\Delta H_{NU}(1-(T/T_m)) - \Delta C_{p,NU}((T_m - T) + T \ln(T/T_m)))/RT}}{1 + e^{-(\Delta H_{NU}(1-(T/T_m)) - \Delta C_{p,NU}((T_m - T) + T \ln(T/T_m)))/RT}} \quad (9)$$

where T_m is the transition temperature, ΔH and ΔC_p are, respectively, the enthalpy and specific heat capacity of denaturation at T_m, and the other terms have the same meaning as in eq 1. After this fitting, the fluorescence and circular dichroism data were converted to apparent unfolded fraction using eq 3 and then globally fitted to a three-state (A, B, and C) model (*25*) using eqs 4, 5, 6, 10, and 11:

$$\Delta G_{AB} = \Delta H_{AB}(1 - T/T_{m,AB}) - \Delta C_{p,AB}\{(T_{m,AB} - T) + T \ln (T/T_{m,AB})\} \quad (10)$$

$$\Delta G_{BC} = \Delta H_{BC}(1 - T/T_{m,BC}) - \Delta C_{p,BC}\{(T_{m,BC} - T) + T \ln (T/T_{m,BC})\} \quad (11)$$

Influence of Electrostatic Interactions on the Relative Stability of the Three States. The stability of the scFv is pH dependent. We have analyzed the influence of pH on the relative stability of the scFv A, B, and C states using an approach inspired in the analysis of the relative integrity of hydrogen bonds in native and partly denatured apoflavodoxin (*27*). This analysis makes use of the Φ concept to describe equilibrium intermediates (*27*). The difference between the free energy of the AB equilibrium at a given pH value and that at a reference pH value (pH 9.3 is used, although the conclusions are not affected by the reference pH) is calculated using eq 12:

$$\Delta\Delta G_{AB} = \Delta S_{AB(pH9.3)}\Delta T_{m,AB(pH-pH9.3)} \quad (12)$$

and, similarly, the corresponding difference for the BC equilibrium is

$$\Delta\Delta G_{BC} = \Delta S_{BC(pH9.3)}\Delta T_{m,BC(pH-pH9.3)} \quad (13)$$

When the protein solution pH is changed from any given reference pH, the ionization state of several protein residues will change. These simultaneous charge mutations modify electrostatic interactions all over the protein and may alter its conformational stability. The degree by which the modified electrostatic interactions of A (absent in C) are present in B can be probed by comparing the stability effects of the pH change in the free energy of the BC and AC equilibria. The Φ parameter reports on the overall integrity in B of the modified electrostatic interactions:

$$\Phi = \frac{\Delta\Delta G_{BC}}{\Delta\Delta G_{AC}} \quad (14)$$

where

$$\Delta\Delta G_{AC} = \Delta\Delta G_{AB} + \Delta\Delta G_{BC} \quad (15)$$

A Φ value of 1 indicates that the electrostatic interactions in B are similar to those in A, while a value of 0 indicates they are similar to those in the C state.

scFv Modeling and Calculation of Tryptophan Solvent Exposure. A preliminary framework structure of the anti-HBsAg scFv was generated using the Homology module of InsightII (MSI Inc.) to fit the anti-HBsAg scFv sequence into the coordinates of PDB 4fab V_H domain and of PDB 1sbs V_L domain. Each domain model was separately refined by 10 000 cycles of steepest descent energy minimization followed by 12 000 cycles of conjugate gradient energy minimization using CHARMm (*28, 29*). The heavy- and light-chain CDRs were further modeled using a knowledge-based approach to search for suitable structures (*30*−*35*) with the Homology module of InsightII (MSI Inc.). The six loops generated were spliced onto the framework structure, and the resulting domain models were energy-minimized with CHARMm and superimposed onto the V_H and V_L domains of McPC603 (*36*) (PDB code: 1mpc). The structure was then subjected to limited energy minimization at the domain/domain interface to alleviate unfavorable van der Waals contacts. The solvent-accessible surfaces of the tryptophan residues in the modeled Fv fragment were calculated with InsightII, using a 1.4 Å probe radius and standard van der Waals radii (*37*). All calculations were performed on a Silicon Graphics workstation.

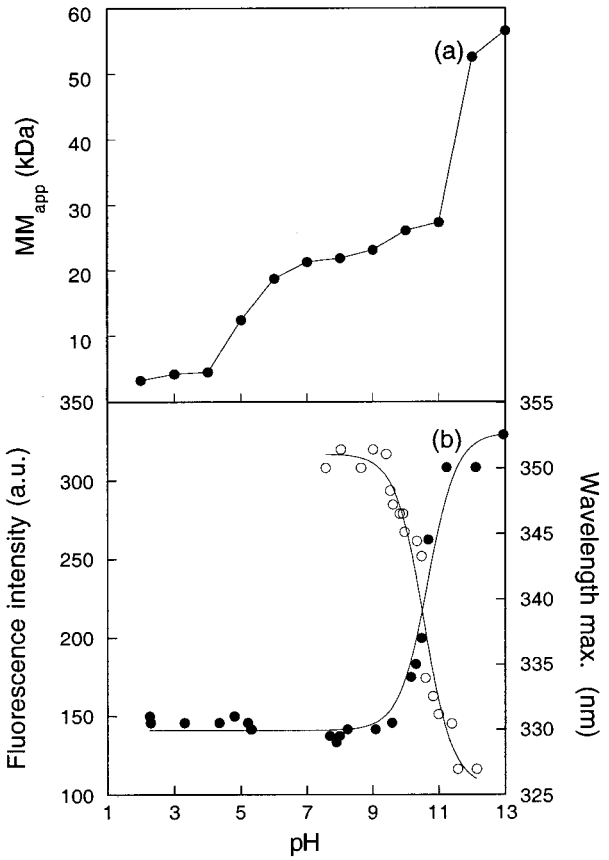

FIGURE 1: pH dependence of (a) the apparent molecular mass and (b) the fluorescence intensity (open circles) and wavelength of maximal fluorescence emission (closed circles) of the anti-HBsAg scFv fragment. A 55 μM solution of the scFv fragment in 2 mM boric acid, 2 mM sodium phosphate, 2 mM sodium citrate, and 100 mM NaCl at different pH values was used for the gel filtration experiments. The temperature was 25 ± 2 °C. In the fluorescence experiments, the scFv concentration was 1 μM, and it was dissolved in the same buffer but with 25 mM NaCl.

RESULTS

Conformation of Anti-HBsAg as a Function of pH. Size exclusion chromatography is a simple way to assess the state of aggregation of protein solutions. The anti-HBsAg scFv was eluted from an exclusion chromatography column as a single peak, from pH 7 to 13. The variation of the apparent molecular mass of the major or single peak from pH 2 to 13 is shown in Figure 1a. In the 7−11 pH interval, the apparent molecular mass is close to the theoretical value of 27.9 kDa.

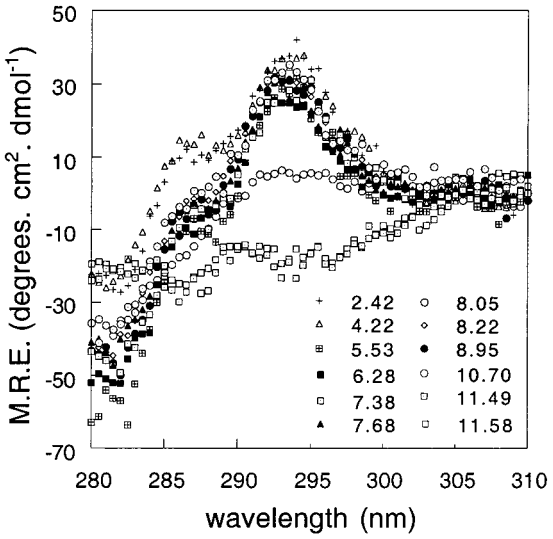

FIGURE 2: scFv near-UV CD spectrum at different pH values. The spectra were recorded at 25.0 ± 0.1 °C using a protein concentration of 10 μM in a 2 mM boric acid, 2 mM sodium phosphate, 2 mM sodium citrate, and 25 mM NaCl buffer.

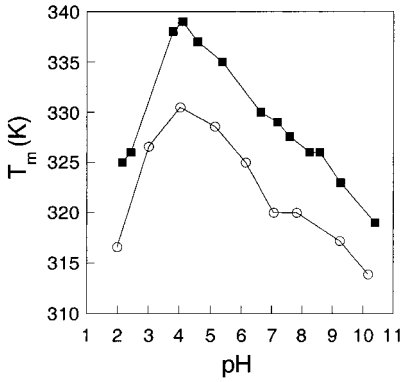

FIGURE 3: pH dependence of the scFv apparent T_m as determined from fluorescence and far-UV CD experiments. The thermal unfolding data (fluorescence or CD) at different pH values were fitted to a simple two-state model, and the T_ms calculated are represented. Open circles: fluorescence; closed squares: far-UV CD. Protein concentration was 1 μM and the buffer: 2 mM boric acid, 2 mM sodium phosphate, 2 mM sodium citrate, and 25 mM NaCl buffer. For the far-UV CD curves, the concentration of the buffering salts was 1 mM.

At higher pH values, the apparent molecular mass sharply increases, reflecting alkaline denaturation. Below pH 6, the protein is partly retained in the column, which gives rise to very low apparent molecular masses, probably reflecting scFv aggregation at low pH values.

The fluorescence intensity and the wavelength of maximal fluorescence emission of the scFv are shown in Figure 1b as a function of pH. Below pH 9, the emission maximum stays at 330 nm, but at higher pH values, there is a sharp transition to around 353 nm with an apparent pK_a of 10.7. At high pH, the tryptophan residues in the scFv are thus fully exposed to solvent. The exposure is accompanied by a concomitant decrease of fluorescence intensity with almost the same apparent pK_a (10.6).

The scFv near-UV CD spectrum (Figure 2) displays a positive peak centered at 294 nm. The intensity of the peak, characteristic of aromatic residues in asymmetric environments usually associated with native conformations (*38*), is similar in the 2−10 pH interval, but levels off at higher pH values. Below pH 5.5, a shoulder appears at 287 nm.

Three pH regions can thus be deduced from the size exclusion chromatography and spectroscopic data, where the scFv adopts different conformations. Below pH 6.5, the protein is probably aggregated. Since the near-UV CD peak at 294 nm is still observed, and even a new peak at 287 nm appears, it seems that the native conformation is retained in the aggregates. In the 7−9 pH interval, the scFv is monomeric; the emission maximum wavelength indicates a compact conformation; the far-UV CD spectrum (Figure 6) shows a minimum at 215 nm, as expected for a β protein; and the near-UV CD spectrum displays a distinct peak, which is characteristic of well-folded protein conformations. In addition to being monomeric, the protein is thus well-folded in the 7−9 pH interval. In fact, the scFv displays its biological activity from, at least, pH 7.1 to pH 9.3 (*17*, *18*). Above pH 11, the apparent molecular mass is consistent with the expected volume of the scFv unfolded state (*20*) but also with that of the scFv dimer. The emission maximum, however (*39*), indicates that the protein is fully denatured at high pH. The alkaline denaturation is manifested by a sharp increase in the fluorescence emission maximum and a concomitant marked decrease in the quantum yield of the tryptophan residues. In addition, the near-UV CD peak at 294 nm, characteristic of the native conformation, disappears.

Equilibrium Thermal Denaturation of scFv at Different pHs. The scFv thermal unfolding transition at different pH values (from 2.2 to 10.4) was monitored by fluorescence emission intensity and far-UV circular dichroism, and the apparent temperatures of mid denaturation (shown in Figure 3) were calculated (using eq 9) from fits to the simple two-state model. No thermal transition is observed above pH 11 (data not shown). At the micromolar protein concentration of these experiments, the stability increases from pH 2 to a maximum at around pH 4, and then decreases toward the alkaline region. Interestingly, there is a large and consistent difference in the T_m calculated, at any given pH, from the fluorescence and from the CD curves. The noncoincidence of protein unfolding curves monitored following different spectroscopic properties is classical evidence of the accumulation of an equilibrium intermediate in the unfolding (*24*, *25*, *27*, *40*−*42*).

Before proceeding to a thorough analysis of the scFv unfolding equilibrium at pH 7.0, we have investigated whether the thermal denaturation is reversible at this pH. Our near-UV CD data indicate that the spectrum of the native conformation (Figure 2), lost at high temperature, is slowly but fully recovered after cooling (in about 7 h, not shown). In addition, since a slow equilibration can sometimes compromise the proper thermodynamic analysis of conformational equilibria, we have checked that, in our denaturation experiments, the protein solution remains at equilibrium. To that end, we have performed, at pH 7.0, thermal denaturations at different heating rates (from 0.1 to 0.8 °C min^{-1}), and the same T_m has been obtained in all cases, which allows a meaningful thermodynamic analysis of the curves (see ref *43* for a full discussion). Finally, since the apparent stability of proteins is markedly dependent on the state of aggregation (*44*), the pH interval where the protein remains monomeric at the protein concentration used for the thermal unfolding experiments (1−4 μM) has been determined by recording, at each pH value, thermal unfolding curves at different

Table 1: Thermodynamic Parameters for the Three-State Thermal Unfolding of Anti-HBsAg scFv and Spectroscopic Properties of the Intermediate State[a]

pH	ΔH_{AB} (kcal mol^{-1})	$T_{m,AB}$ (K)	ΔH_{BC} (kcal mol^{-1})	$T_{m,BC}$ (K)	Z_{fluor}	$Z_{farUV\ CD}$	$Z_{nearUV\ CD}$
6.63	177 ± 13	322 ± 0.1	154 ±20	331 ± 0.2	1.00 ± 0.03	0.02 ± 0.06	−
7.19[b]	123 ± 4	322 ± 0.1	115 ± 12	330 ± 0.2	0.98 ± 0.01	0.22 ± 0.04	
	121 ± 2	322 ± 0.1	119 ± 6	330 ± 0.1	0.98 ± 0.01	0.20 ± 0.02	0.05 ± 0.02
7.59	86 ± 4	321 ± 0.2	117 ± 5	328 ± 0.1	0.98 ± 0.03	0.11 ± 0.02	−
8.59	95 ± 8	321 ± 0.3	121 ± 19	327 ± 0.3	1.00 ± 0.05	0.23 ± 0.06	−
9.27	116 ± 5	317 ± 0.2	107 ± 11	324 ± 0.2	0.95 ± 0.03	0.14 ± 0.04	−

[a] Fluorescence intensity and far-UV CD thermal unfolding curves were globally fitted to a three-state model (see Materials and Methods). Errors provided by the fitting program. [b] The data in the lower row correspond to a global analysis that, in addition to the fluorescence intensity and far-UV CD thermal unfolding curves, included a near-UV CD thermal unfolding curve.

protein concentrations. In the 6.3−9.3 pH interval, no protein concentration effect on scFv stability was noticed at scFv concentrations below 4 μM (not shown). At lower pH values, the apparent stability was concentration dependent, and at higher pH values, the denaturation was not reversible. The anti-HBsAg scFv, in the 6.3−9.3 pH interval and at 4 μM or lower concentrations, is therefore a monomer that experiences a reversible thermal unfolding. At pH 7.0, the scFv remains monomeric at a 10 μM concentration (Figure 4a).

Because the noncoincidence of the fluorescence and CD unfolding curves (see T_ms in Figure 3) indicates the accumulation of an intermediate, we have performed a global three-state analysis of the thermal unfolding data (fluorescence and far-UV CD) in the 6.3−9.3 pH interval. At pH 7, the analysis includes, additionally, near-UV CD unfolding data. In these three-state analyses (*25*), all thermodynamic properties of the two equilibria, A−B and B−C, are globally constrained, but the degree of spectroscopic resemblance between the B state and the C state (described by the *Z* parameter; see Materials and Methods) is allowed to vary among the different techniques used to monitor the unfolding. The thermodynamic parameters of the A−B and B−C equilibria, derived from the global fit, are listed in Table 1 and a representative of the data at pH 7.0 (raw data and globally fitted data) is shown in Figure 5. As the transitions are sharp and well separated by around 8 °C, the calculated transition temperatures of the two equilibria roughly reflect those obtained from simple two-state fits of the fluorescence curve (A−B equilibrium) and of the near- and far-UV CD curves (B−C equilibrium). At the temperature of maximal intermediate accumulation (327 K at pH 7.0), the B state represents around 85% of the scFv molecules (not shown). The *Z* values (see Table 1) indicate that the emission fluorescence intensity of B is like that of the C state, while its far-UV CD ellipticity is close to that of A (native). At pH 7, where near-UV CD data have been included in the global analysis, the intermediate near-UV CD ellipticity is also native.

Figure 5 shows, in addition, the temperature dependence of the wavelength of maximal emission, a parameter that has been used (*11, 16*) to follow the unfolding of different scFv molecules. As the temperature is raised, the fluorescence maximum of the anti-HBsAg scFv sharply increases to 335 nm roughly following the A−B transition and then keeps increasing at higher temperatures, even when the B−C transition is finished. This indicates the C state is not fully unfolded. Additional evidence comes from the far-UV CD spectrum at 60 °C (Figure 6), which is not consistent with a fully denatured conformation.

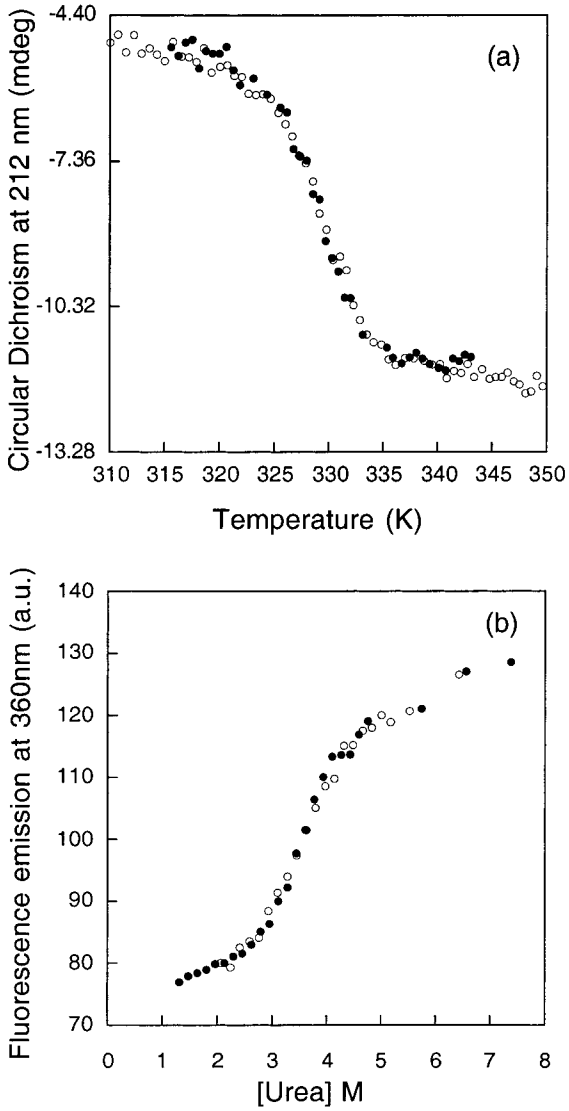

FIGURE 4: Protein concentration independence of the thermal and urea denaturations of scFv. (a) Thermal denaturation of scFv at pH 7.0 followed by far-UV CD using 1 μM (closed circles) and 10 μM (open circles) protein concentrations in 1 cm and 1 mm cuvettes, respectively. (b) Urea denaturation of scFv at pH 7.0 followed by fluorescence intensity using 1 μM (closed circles) and 4 μM (open circles) protein concentrations. The 1 μM curved shown (*Y*) is related to the original one (*X*) by: $Y = 36 + 0.67X$.

Equilibrium Urea Denaturation of scFv at Neutral pH. The anti-HbsAg scFv can also be unfolded by urea, and the conformational change is conveniently followed using emission fluorescence or far-UV CD (Figure 7). To avoid urea interference, the CD change was followed at 231 nm. As in

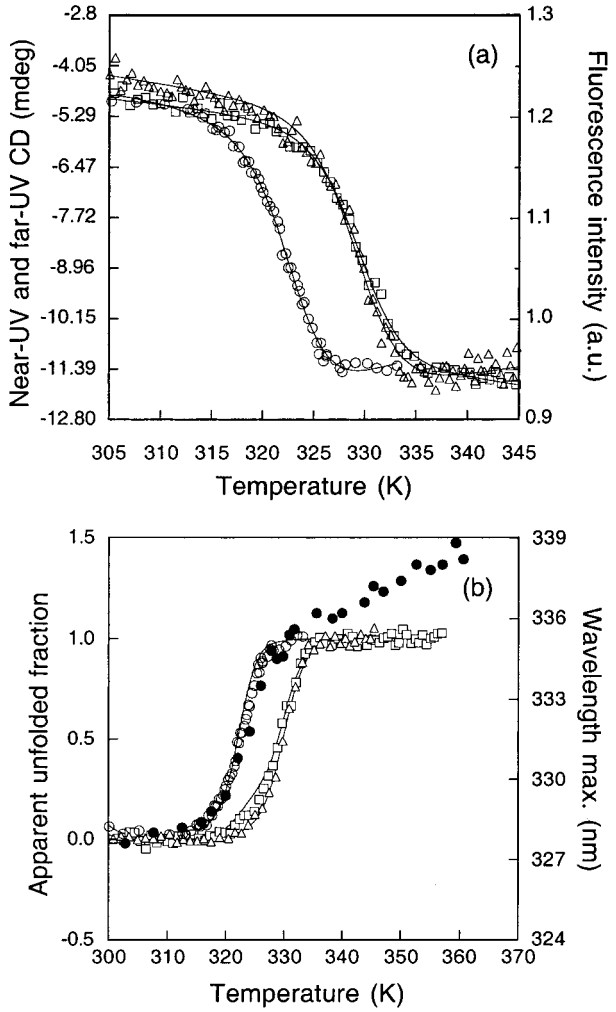

FIGURE 5: Thermal denaturation of scFv at pH 7.0, followed by fluorescence intensity (open circles), far-UV CD (open squares), near-UV CD (open triangles), and wavelength of maximal fluorescence emission (closed circles). (a) Raw data. The near-UV CD curve shown (Y) is related to the original one (X) by $Y = -11.4 + 9.9X$. The solid lines are individual fits to the two-state model. (b) The fluorescence intensity, far-UV CD, and near-UV CD data were globally fitted to a three-state model (see Materials and Methods and ref *27*). The apparent fraction of folded scFv fragment is represented. The solid lines are the global fit to the three-state model. Protein concentration was 1 μM for the fluorescence and far-UV CD curves and 10 μM for the near-UV CD curve.

the analysis of the thermal unfolding curves, the fluorescence and CD urea unfolding curves at neutral pH were first independently fitted to a simple two-state model, and the corresponding urea concentrations of mid-denaturation obtained were found to be significantly different for the two techniques (3.49 M for fluorescence and 3.80 M for DC; Figure 7a). This indicates that an intermediate accumulates in the urea unfolding, as already observed in the thermal unfolding. We then determined that the scFv stability was protein concentration independent below 4 μM (Figure 4b), and then we tested for reversibility by diluting an scFv solution, previously unfolded with urea. The native fluorescence and near-UV CD spectra were fully, although slowly, recovered. In addition, and for the reason discussed in the preceding thermal unfolding section, we checked that the unfolding solutions had attained equilibrium when the fluorescence or CD signals were acquired by recording urea unfolding curves after different incubation times, and no

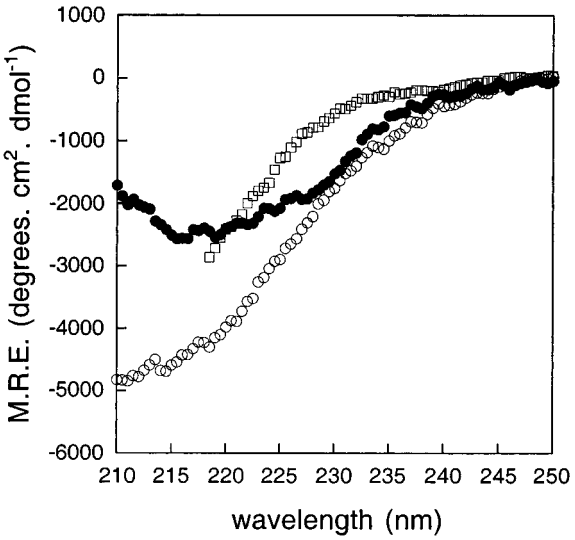

FIGURE 6: Far-UV CD spectrum of scFv at pH 7.0, in different conditions. A 1 μM scFv solution was used. Closed circles: 25.0 $\pm$ 0.1 °C; open circles: 60.0 $\pm$ 0.1 °C; open squares: 25.0 $\pm$ 0.1 °C plus 5 M urea.

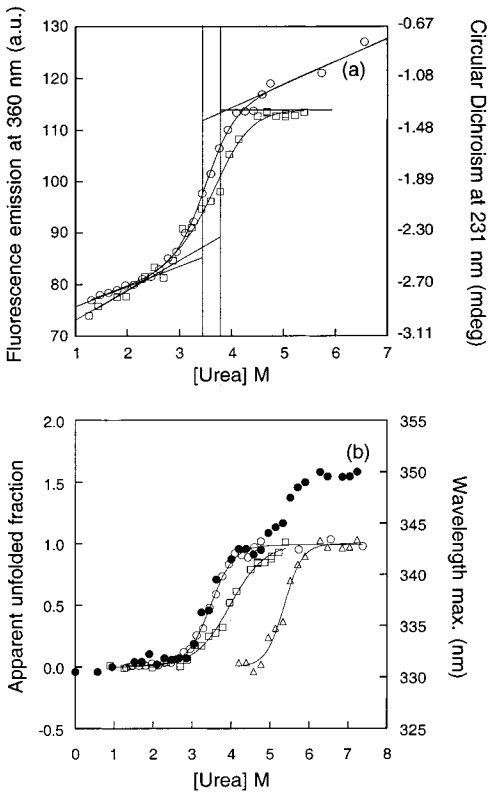

FIGURE 7: Urea denaturation of scFv at pH 7.0, followed by fluorescence intensity (open circles), far-UV CD (open squares), and wavelength of maximal fluorescence emission (closed circles). (a) Raw data fitted to a simple two-state equation. The slopes of the native and denatured baselines are represented. The vertical lines indicate the urea concentrations of half-denaturation. (b) The fluorescence intensity and far-UV CD data were globally fitted to a three-state model (see Materials and Methods). The apparent fraction of unfolded scFv fragment is represented. The solid lines are the global fit to the three-state model. The wavelength red-shift occurring at higher urea concentration is additionally represented for better comparison (open triangles), fitted to a two-state equation. Protein concentration was 1 μM.

differences in the curves were noticed. Finally, we performed the global fit of the fluorescence and CD data to the three-

Table 2: Thermodynamic Parameters for the Three-State Urea Unfolding of Anti-HBsAg scFv at Neutral pH, and Spectroscopic Properties of the Intermediate[a]

$\Delta G_{w,AB}$ (kcal mol^{-1})	m_{AB} (kcal mol^{-1} M^{-1})	$U_{1/2,AB}$ (M)	$\Delta G_{w,BC}$ (kcal mol^{-1})	m_{BC} (kcal mol^{-1} M^{-1})	$U_{1/2,BC}$ (M)	Z_{fluor}	$Z_{farUV\ CD}$
5.51 ± 0.37	1.58 ± 0.12	3.49	6.16 ± 1.17	1.44 ± 0.23	4.28	0.93 ± 0.05	0.40 ± 0.08

[a] Fluorescence intensity and far-UV CD urea unfolding curves were globally fitted to a three-state model (see Materials and Methods). Errors provided by the fitting program.

state model (see Materials and Methods). The results of the global analysis are shown in Table 2 and in Figure 7b. The maximal intermediate accumulation (around 55%) occurs near 4.0 M urea. The B state displays emission fluorescence intensity close to the C state and a far-UV signal closer to the native A state than to the C state.

In Figure 7b, the urea dependence of the wavelength of maximal emission is also shown. There are two clear, cooperative, red-shift steps. The first one mimics the fluorescence intensity transition. The second one takes place when the CD transition is almost finished. This second red-shift transition, from 343 to 350 nm, indicates that the C state is, actually, an intermediate conformation that can be cooperatively denatured by urea. Since this high urea red-shift transition is well-separated from the lower urea CD transition, the energetics of the equilibrium involving the C state and the fully denatured state (D) can be approximated by a two-state analysis of the high urea red-shift transition (although analyzing wavelength shifts only provides estimates of the real values). This analysis indicates the free energy difference between the C and D states is around 13 kcal mol^{-1}, with an *m* slope of 2.4 ± 0.5 kcal mol^{-1} M^{-1}, indicative of significant hydrophobic side chain burial in C relative to the denatured state. The slope *m* in denaturant unfolding transitions has been related to protein size (*45*). The overall change determined for the A−D transition in the scFv fragment is 5.5 ± 0.9, which is higher than the highest value of 3.7 expected from its size and the spread of data in Figure 2B of reference *45*. The discrepancy may be related to the fact that the data concerning the C−D transition are only an approximation because a spectral wavelength shift rather than an intensity change has been analyzed. Alternatively, it is possible that the correlation observed between *m* values and size in proteins displaying simpler equilibria does not hold always for more complex proteins.

Anti-HBsAg scFv Model and Tryptophan Accessibility. Sequence comparison of the anti-HBsAg scFv with inmunoglobulins of known crystal structure provided suitable templates for the variable regions of the anti-HBsAg scFv. The L chain of anti-human chorionic gonadotropin (pdb code: 1sbs) was 87% identical to the scFv at the V_L domain, with a one-residue insertion in the CDR3. On the other hand, the H chain of a fluorescein−Fab complex (pdb code: 4fab) displayed a 74% homology with the scFv at the V_H, with a three-residue deletion in the CDR3. The CDRs, that constitute the less conserved regions, were further modeled by loop searching.

The stability and fluorescence properties of different scFv antibody fragments derived from McPc603 (*36*) and from 4D5-8 (*46*) have been characterized in depth (*10, 12*). Our model of the anti-HBsAg scFv is shown in Figure 8 superimposed to that of the Fv region of 4D5-8 (*46*) (pdb code: 1fvc). The two structures are very similar. The overall

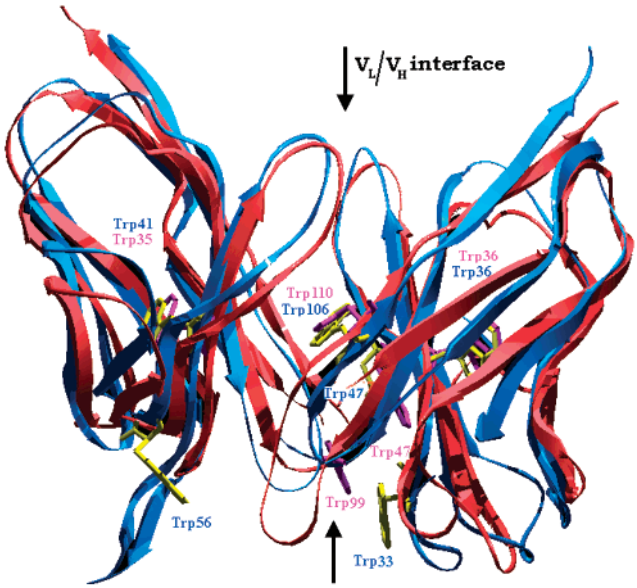

FIGURE 8: Modeled structure of the anti-HBsAg scFv fragment (cyan; Trp residues in yellow) superimposed on the structure of 4D5-8 scFv (orange; Trp residues in pink; pdb code: 1fvc). The interface of the V_L and V_H domains is indicated with arrows.

root-mean-square deviations for the backbone atoms of the aligned positions of 4D5-8 and the scFv, including the conserved β-sheet framework residues and the hypervariable regions, were 1.6 Å. A comparison of the two structures shows that the only Trp residue in the 4D5-8 V_L domain (Trp41) is conserved in the anti-HBsAg scFv, but this single-chain fragment contains one additional Trp residue at position 56. In the V_L domain, either molecule displays four tryptophan residues, three of which are conserved (Trp36, -47, and -106 in the anti-HBsAg scFv). The fourth Trp residue in this scFv V_H (Trp33) is located close to the position of Trp99 in the 4D5-8 V_H domain. The solvent accessibilities of the Trp side chains in the anti-HBsAg scFv are compared in Table 3 to those of the corresponding Trp residues in 4D5-8 and in McP603.

DISCUSSION

Four-State Thermal Unfolding of Anti-HBsAg scFv. Thermal denaturation studies of scFvs have been hampered by the tendency of these molecules to aggregate upon unfolding at high temperature. Using a 10 μM protein concentration and light scattering detection, Wörn and Plückthun (*16*) studied the thermal unfolding of a number of variants of an scFv antibody fragment that aggregated at different temperatures that correlated to their conformational stability. Differential scanning calorimetry has also been used to study the unfolding of an anti-ferritin scFv (*47*). These authors described a two-state scFv thermal unfolding, but, at the concentration used (40 μM and above), the unfolding was irreversible. It seems, thus, that in order to be able to

Table 3: Solvent Accessibilities of the Tryptophan Residues in the V_L and V_H Domains of Anti-HBsAg scFv,[a] 4D5,[b] and McPc603[c] scFvs

	anti-HBsAg scFv			4D5			McP603		
		accessibility (%)			accessibility (%)			accessibility (%)	
domain	residue	in isolated domain	in V_LV_H complex	residue	in isolated domain	in V_LV_H complex	residue	in isolated domain	in V_LV_H complex
V_L	Trp41	0	0	Trp35	0	0	Trp41	0	0
	Trp56	33	25						
V_H	Trp33	39	22	Trp99	27	17	Trp107	48	27
	Trp36	0	0	Trp 36	0	0	Trp36	0	0
	Trp47	38	20	Trp 47	37	4	Trp47	42	1
	Trp106	28	8	Trp 110	35	10	Trp112	36	2

[a] Calculated from the modeled structure (based on the V_H domain in 4fab and the V_L domain in 1sbs). [b] Calculated from PDB code: 1fvc. [c] Calculated from PDB code: 1mpv.

characterize the thermal unfolding of scFv molecules, low protein concentrations should be used, and a careful evaluation of the aggregation state of the protein at the pH used and of the reversibility of the thermal transition is needed. We have determined (see Results) that, in the 6.3−9.3 pH interval and at protein concentrations of 4 μM or lower, the anti-HBsAg scFv is monomeric and experiences reversible thermal denaturation. At pH 7.0, the scFv remains monomeric at 10 μM (Figure 4a). It is thus an appropriate model to perform a thorough characterization of the thermal unfolding equilibrium. The following discussion on the thermal unfolding equilibrium refers to solution conditions where the scFv is monomeric and the unfolding reversible.

A main issue is to establish the minimal model that describes the unfolding. To that end, we have monitored the thermal unfolding by two different techniques and found that the curves cannot be superimposed. This is classical evidence of the accumulation of an equilibrium intermediate. We have thus performed a global three-state analysis of the fluorescence and far-UV CD data, as described (*25*, *27*). In addition, we have noticed that the wavelength of the maximum fluorescence emission (336 nm) displayed by the C state (Figure 5b; see Results) indicates it is not fully denatured. Therefore, a forth state (D: denatured) is required to explain the overall equilibrium.

(A) The First Thermal Unfolding Transition. State A = Native (N); State B = First Intermediate (I_1). The calculated T_m values at different pHs for the N−I_1 equilibrium in the three-state analysis are very similar to those determined from the simple two-state fits of individual curves because the first transition is well separated from the higher temperature one (monitored by CD). As judged from the T_m values, the stability of the native state slowly declines as the pH increases from 6.6, while the enthalpy change does not vary much with pH. The *Z* parameters (see Materials and Methods) clearly indicate that the secondary structure content of I_1 is similar to that of the native state while its fluorescence resembles that of the C, more unfolded, state. The equilibrium thermal unfolding has also been investigated at pH 7.2 by near-UV CD. This transition mimics the far-UV CD one and gives rise to a *Z* parameter that indicates the near-UV CD spectrum of I_1 is native-like. This, together with the small change in secondary structure and the relatively small fluorescence wavelength shift, indicates a limited departure from the native conformation. Two possible conformations of I_1 consistent with the data available are the following: (1) the domains are dissociated but remain essentially native; (2) one domain (giving rise to all of the near-UV CD signal of the scFv) is native, and the other is in a molten globule conformation that retains most of the secondary structure.

(B) The Second Thermal Unfolding Transition. State B = First Intermediate (I_1); State C = Second Intermediate (I_2). The pH dependence of the second transition, I_1−I_2, is quite similar to that of the first one. The stability of I_2 declines as the pH increases from 6.6, and the enthalpy change does not vary much with pH. Some insight into the structure of I_2 can be obtained from the spectroscopic data. The loss in I_2 of the near-UV CD signal indicates that at least one of the domains (in fact any of the two domains that happens to contribute to the spectrum) is either unfolded or in a molten globule conformation. There are, however, clear indications that I_2 is not fully unfolded. First, its far-UV CD spectrum is peculiar (Figure 6): it is more pronounced than that of the native state. Second, the wavelength of maximal emission fluorescence at 332 K (where the three-state analysis indicates that 85% of the scFv molecules are already in the I_2 state) is of 336 nm, very far from typical of fully unfolded proteins. In fact, the very small shift in the wavelength of maximal emission concomitant with the I_1−I_2 transition suggests that no global unfolding of any of the domains occurs in this step.

(C) The Third Thermal Unfolding Transition. State C = Second Intermediate (I_2); State D = Denatured State. Increasing the temperature from 332 to 360 K slowly shifts the wavelength of maximum emission to the red. As shown in Figure 5b, the emission maximum (that at lower temperatures sharply increases, roughly mimicking the N-to-I_1 transition) sluggishly increases from 336 to 339 nm, still far from the typical 355 nm of tryptophan-containing fully unfolded proteins. Since changes in the wavelength of maximum emission constitute clear indications of a higher exposure of tryptophan residues to solvent, the observed shift cannot be considered a simple baseline drift. We interpret these facts as indicating that I_2 is a compact state that can be further unfolded in a noncooperative fashion.

The minimal model for the thermal unfolding of this scFv is thus

$$N \leftrightarrow I_1 \leftrightarrow I_2 \leftrightarrow D$$

where N represents the native state, I_1 is an intermediate with altered fluorescence properties (lower intensity and red-shifted maximum) but close to native secondary structure and native aromatic tertiary interactions, I_2 is a compact state

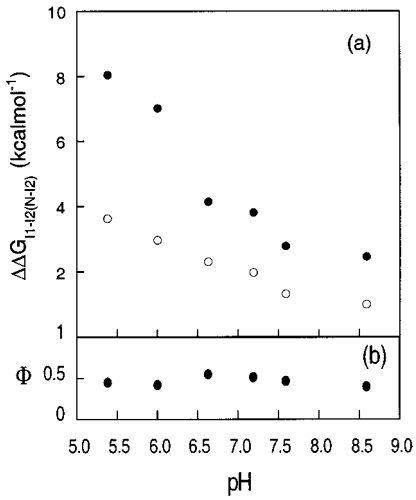

FIGURE 9: ϕ-analysis of the electrostatic interactions in native, I_1, and I_2 scFv thermal intermediates. (a) Free energy differences of the I_1-I_2 and $N-I_2$ thermal unfolding equilibria at different pH values (referenced to pH 9.0). (b) ϕ-values (see Materials and Methods and Discussion), indicative of the overall integrity of electrostatic interactions in I_1 (relative to N and to I_2).

with non-native secondary structure and no sign of well-defined interactions involving aromatic residues, and D is the unfolded state. Between N and I_1, and between I_1 and I_2, there are clear energetic barriers, while between I_1 and D there are not, or they are small. In this respect, the I_2 intermediate resembles a compact denatured state.

Integrity of Electrostatic Interactions in the scFv Thermal Intermediates. When the energetics of a conformational equilibrium involving more than two species (transient or not) are well-characterized, the effect of protein structure perturbations on the relative stability of the different states may be used to derive hints on the structure of the intermediate conformations. This approach has been recently exemplified in the analysis of hydrogen bonding in an apoflavodoxin equilibrium thermal intermediate (*27*). In that work, the perturbation used was the mutation of side chain residues, as originally devised to analyze the structure of folding intermediates and transition states (*48*). We propose here a different approach where the perturbation is simply a pH change from a given reference pH. A change in the pH of a protein solution represents the simultaneous introduction of many mutations (partial ones if the pH change is small) consisting of proton binding or release, plus any associated structural change (not expected to be large within the pH interval where the native conformation is dominant). It is clear that an interpretation of these changes may not achieve the same atomic resolution as a mutational analysis, but it can be appropriate to describe the relative contribution of electrostatic interactions to the energetics of the different conformations.

The effect of a pH change on the stability difference of the $N-I_1$ (A−B) and I_1-I_2 (B−C) equilibria is calculated from eqs 12 and 13, and the effect on the overall $N-I_2$ equilibrium can be obtained by adding the two quantities. Figure 9a shows the free energies of the $N-I_2$ and I_1-I_2 equilibria as a function of pH (taking pH 9.3 as an arbitrary reference: ΔG_{I1-I2}(pH 9.3) = 0 and ΔG_{N-I2}(pH 9.3) = 0. The differential free energies of the equilibria increase toward acidic pHs. When these differential energies (that represent the perturbation of the free energies on changing the pH) are compared, a Φ parameter can be calculated (see Materials and Methods) that estimates the degree by which the electrostatic interactions present in the native state and absent in the I_2 state are formed in I_1. A remarkable constancy of the Φ value (Figure 9b) is obtained in the whole pH interval analyzed (that includes pH values below pH 6.5 where the scFv is not monomeric), suggesting the conformations of the native and I_1 states are not markedly altered upon association at low pH. The constancy of the Φ value also suggests, although does not prove, that the same three states (N, I_1, and I_2) are present in the pH interval analyzed. Φ values of 1 would indicate that the electrostatic interactions probed are totally formed in the intermediate, while Φ = 0 would mean the interactions are as broken in I_1 as in I_2 (*27*). The Φ value obtained (around 0.4) indicates that the electrostatic interactions contributing to the stability of the native state relative to I_2 are partly formed in I_1 (around 40%) and that this holds in a wide pH interval. A Φ value of around 0.4 is consistent with either of the two possible conformations proposed for I_1 because it can reveal either that there is a general debilitation of the electrostatic interactions all over the scFv (as a consequence of domain−domain dissociation), or simply that one domain displays native interactions and the other one more unfolded interactions similar to those present in I_2.

Four-State Urea Unfolding of Anti-HBsAg scFv at Neutral pH. Chemical denaturation studies of several scFv fragments have been reported (*4*, *9*−*12*, *16*). In several instances, fluorescence intensity unfolding curves have been fitted to two-state models, and fair fittings to the experimental data have been obtained. It should be pointed out, however, that it is not unusual, in the equilibrium unfolding of proteins, that individual unfolding curves obtained by monitoring one particular property display the typical sigmoidal shape associated with two-state processes, and yet the accumulation of an intermediate may be evidenced by using additional techniques (*27*). In this respect, the superposition of unfolded curves recorded by monitoring different protein properties is a standard criterion to invoke two-state mechanisms (*49*, *50*). Recent studies by Wörn and Plückthun (*11*, *16*) have proved that some scFv fragments display a more complex chemical denaturation behavior by following the change in wavelength of maximal fluorescence emission as a function of denaturant concentration.

From a practical point of view, the 'relevant' conformational stability of a protein may be defined as the difference in free energy between the native state and that of the most stable non-native intermediate at equilibrium (*51*). It thus seems important to obtain a full picture of the scFv unfolding equilibrium in order to calculate this stability difference. To that end, we have studied the urea unfolding of the scFv under solution conditions where the unfolding is fully reversible and protein concentration independent (pH 7.0, protein concentration below 4 μM, 25 °C). Similarly to what occurs in the thermal denaturation, urea unfolding curves followed by different techniques (Figure 7) cannot be superimposed (they yield significantly different half-urea values when fitted to simple two-state equations), revealing the presence of an equilibrium intermediate in the chemical denaturation. Additionally, the wavelength of maximal emission of the C state is far from the typical value of

unfolded polypeptides. The minimal model consistent with the urea unfolding data is thus four-state. In the following discussion, we do not prejudge the intermediates in the chemical denaturation are equivalent to those found in the thermal denaturation. In fact, it seems they are not.

(A) The First Chemical Unfolding Transition. State A = Native (N); State B = First Intermediate (I_1). According to the global fit in Table 2, the N−I_1 energy gap is around 5.5 kcal mol^{-1}. The cooperativity of the urea transition (reflected in the *m* value) indicates that the hydrophobic residues of I_1 are more exposed to solvent than in the native state. As for the spectroscopic properties of I_1, the *Z* parameters indicate its fluorescence intensity is similar to that of the C state accumulating at higher urea concentrations, while the CD spectrum is closer to native than to the C state.

(B) The Second Chemical Unfolding Transition. State B = First Intermediate (I_1); State C = Second Intermediate (I_2). The energy gap between I_1 and I_2 (around 6 kcal mol^{-1}) is similar to that between N and I_1. The *m* value of the urea transition reflects that, in I_2, the hydrophobic residues are more exposed to solvent than in I_1, and the *Z* parameters show that the fluorescence intensity of I_2 is similar to that of I_1 while the CD signal is reduced. Unlike in the thermal unfolding, the far-UV CD spectrum of I_2 is not atypical, and it seems reasonable to assume (see Figure 6) that the secondary structure content is decreased in I_2.

(C) The Third Chemical Unfolding Transition. State C = Second Intermediate (I_2); State D = Denatured State. According to the three-state analysis, 90% of the scFv molecules are in the I_2 state at 4.8 M urea. However, the wavelength of maximal fluorescence emission at that urea concentration is just 343 nm, indicative of a partial burial of tryptophan residues. We have followed the emission maximum at higher urea concentrations and found (Figure 7b) that it keeps increasing up to a stable value of 350 nm at 6 M urea and above. This confirms that the I_2 conformation is, indeed, compact. Looking at the wavelength of maximal emission from 0 to 7 M urea, two transitions are evident, as has been reported for other scFv (*4*, *11*, *12*, *16*). The first one, with a half-urea concentration of around 3.5 M (Figure 7b), perfectly mimics the fluorescence intensity transition associated with the N−I_1 conformational change. The second one, with a half-urea concentration of around 5.5 M urea, is clearly different from the CD transition, associated with the I_1−I_2 transition, and therefore represents a conformational change experienced by I_2. As this second transition is clearly cooperative, it is unlikely to represent a simple expansion of a compact denatured state, and we propose it reflects the unfolding of a compact intermediate (I_2) to a fully denatured state (D). No significant fluorescence intensity change is associated to this transition. This is not too surprising, however, because fluorescence intensity changes in conformational transitions can sometimes be quite small and also because they cannot be easily predicted with the same rational as the shifts in wavelengths.

The minimal scheme for the urea unfolding of the scFv is thus

$$N \leftrightarrow I_1 \leftrightarrow I_2 \leftrightarrow D$$

where N is the native state; I_1 is an intermediate with the same fluorescence intensity as I_2 and D, an emission maximum halfway from native to denatured, and a far-UV CD spectrum closer to N than to I_2; I_2 is a more unfolded intermediate with the same fluorescence intensity than the denatured state, and the same emission maximum as I_1 but with a less intense far-UV CD spectrum (based on the CD spectra and on the unfolding cooperativity, this I_2 chemical intermediate is different from the I_2 thermal intermediate); and D represents the denatured state, with the same fluorescence intensity as I_1 and I_2 but fully exposed tryptophan residues. The CD spectrum of the denatured state has not been characterized due to severe urea interference. The free energy differences of the three urea unfolding equilibria (N−I_1, I_1−I_2, and I_2-D) are around 5.5, 6.0, and 13.0 kcal mol^{-1}, respectively. This indicates that although the N−D energy gap is remarkably large, the relevant conformational stability [that of the N−I_1 equilibrium; (*51*)] is fairly low.

On the Four-State scFv Equilibrium Unfolding: Comparison with Other Fv Fragments. Few thermal denaturation studies of scFv fragments have been reported (*16*, *47*) possibly because of a general tendency of the scFv molecule to aggregate or to experience irreversible thermal denaturation. In contrast with the model presented here, Martsev et al. recently reported (*47*) a two-state scFv thermal unfolding behavior based on a close to unity value of the calorimetric-to-van't Hoff enthalpies obtained in DSC experiments. The denaturation was irreversible, however, and the enthalpy of unfolding very small. We can thus hardly compare our data on the reversible thermal unfolding of the scFv to previous data on other scFv fragments. Comprehensive data on the reversible thermal denaturation of other scFv fragments will have to be gathered to determine whether the model proposed here for the anti-HBsAg scFv fragment is general and, if that is the case, to better define the conformation of I_1 and I_2.

The situation is quite different for scFv chemical denaturation studies where reported data for different scFv fragments abound (*9*, *11*, *12*, *16*, *52*−*54*). In several instances, two-state behavior has been proposed based in the fact that urea or guanidinium unfolding curves followed by fluorescence (intensity or wavelength of maximal emission) can be fitted to a two-state equation. As discussed above, this criterion should be abandoned because mechanisms that are more complex may give rise to apparent two-state unfolding curves if only one technique is used to monitor the unfolding. Clear evidence of more complex mechanisms in scFv chemical unfolding has been provided by Plückthun and co-workers from the two-step red-shift of the fluorescence wavelength of maximum emission upon increasing denaturant concentration (*4*, *11*, *12*, *16*). This group has proposed a model where, depending on the relative strength of the interdomain interactions and on the intrinsic stability of the V_L and V_H domains, scFv unfolding may be sequential. In this model, when the unfolding is sequential, the relative abundance and environment of tryptophan residues in the V_L and V_H domains may give rise, in some cases, to the observed two-step red-shift (reviewed in ref *55*; see also ref *12*). To determine if this model is applicable to the anti-HBsAg scFv fragment, we have modeled its structure (see Materials and Methods and Results). The accessibilities of tryptophan residues in the anti-HBsAg scFv fragment are compared in Table 3 to those of the scFv fragments derived from the 4D5-8 and McPc603 antibodies studied by

Plückthun and co-workers. There is an overall good correspondence between the Trp accessibilities of equivalent tryptophan residues in the three molecules and in their accessibilities in the isolated V_H and V_L domains. As for the Trp residue that is only present in the anti-HBsAg scFv fragment (Trp56 of the V_L domain), its high exposure to solvent precludes it from contributing significantly to a red-shift associated with V_L unfolding. The fluorescence behavior of the anti-HBsAg scFv fragment is thus expected to be similar to that of the 4D5-8 and McPc603 scFvs, unless the relative stabilities of the individual domains or of the domain interface are different.

In the urea unfolding of the anti-HBsAg scFv fragment reported here, a clear two-step red-shift caused by increasing concentrations of denaturant is evident (Figure 7b). According to the scFv classification of Wörn and Plückthun, this indicates that the anti-HBsAg scFv belongs to Class I, where the stability of one domain is far higher than the total stability (intrinsic plus interdomain interactions) of the other. Within this class, a clear step is expected when V_L is the less stable domain, and unfolds at lower denaturant concentration (*16*), while a lower stability of the V_H domain is expected to cause a large initial red-shift followed by a small one associated with V_L unfolding. Based on the fluorescence data and on the resemblance between the anti-HBsAg scFv modeled structure and that of the scFvs studied by Plückthun and co-workers, the anti-HBsAg scFv behavior can be explained if the V_L domain is less stable (interdomain binding energy included) than the V_H domain. The first fluorescence unfolding red-shift step would reflect thus the exposure of the core Trp residue in V_L plus the disruption of the interface, and the second step would correspond to V_H unfolding. According to our interpretation, the V_L domain would be limiting the overall stability of the anti-HBsAg scFv molecule and would therefore be the main target for the rational stabilization of this scFv.

The Wörn/Plückthun model for scFv unfolding implicitly assumes that the unfolding of the individual domains is two-state. However, some deviation from two-state unfolding can be deduced from the fluorescence behavior of, at least, one isolated V_L domain already characterized (see Figure 3a in ref *11*). Because the presence of equilibrium intermediates can pass unnoticed when a single spectroscopic technique is used (*27*), we have combined in this work fluorescence and circular dichroism data (Figure 7). The fluorescence intensity ratio curve (that mimics the first red-shift transition) and the circular dichroism curves cannot be superimposed. This indicates that, as a consequence of the first red-shift-causing unfolding process (that we have attributed to unfolding of the V_L domain), an intermediate appears (I_1) that is transformed, at a higher urea concentration, into a second intermediate (I_2) with reduced secondary structure content. The I_2 intermediate (the native V_H domain, according to our interpretation of the Wörn and Plückthun model) is then fully unfolded at higher urea concentration, giving rise to the second fluorescence red-shift.

Our overall four-state model is thus consistent with the Wörn and Plückthun model but reveals the occurrence of an additional intermediate (I_1) that may contain a partly unfolded V_L domain (perhaps in a molten globule like conformation, as judged by its non-native fluorescence but not far from native secondary structure) while the V_H domain would still be well-folded. At this stage, we cannot ascertain whether the two domains would still be associated in I_1, but the magnitude of the red-shift suggests they would not. The more plausible scenario thus seems that the dissociation of the two domains to form I_1 leaves the weakest domain (V_L) in a partly unfolded conformation that unfolds, at higher urea concentration, with a concomitant loss of secondary structure but no significant fluorescence change, to form I_2. An alternative explanation, that we judge less likely but that cannot be ruled out at present, would attribute the $N-I_1$ transition to a disruption of the domain interface that would dissociate well-folded V_L and V_H domains. In this case, the I_1-I_2 transition would represent the unfolding of a well-folded V_L domain (giving rise to a small, unnoticeable red-shift). In this alternative scenario, the anti-HBsAg scFv would represent a first example of class IV scFv molecules (*16*).

Whatever the details of the intermediate conformations involved, that need further study to be clarified, it is clear that both the urea and the thermal unfolding of the anti-HBsAg scFv fragment are best described by four-state models. An analysis of other scFv fragments by a combination of different spectroscopic techniques is needed to establish whether this is a general property of this family of molecules. An anticipated result of such analyses will be a better understanding of the structure and energetics of scFv equilibrium intermediates, which will in turn help guide the rational stabilization of this increasingly useful family of mini antibodies by focusing on improving the 'relevant' conformational stability.

ACKNOWLEDGMENT

We thank Dr. Jorge Gavilondo, Dr. Marta Ayala, and Mr. Elder Pupo from the CIGB (Centro de Ingeniería Genética y Biotecnología, la Habana, Cuba) for providing us with the anti-HBsAg scFv. We thank Luis A. Campos for helpful discussion and one referee for useful comments.

REFERENCES

1. Berry, M. J., and Pierce, J. J. (1993) Stability of immunoadsorbents comprising antibody fragments. Comparison of Fv fragments and single-chain Fv fragments. *J. Chromatogr. 629*, 161−168.
2. Winter, G., and Milstein, C. C. (1991) Man-made antibodies. *Nature 349*, 293−299.
3. Plückthun, A. (1994) in *Immunochemistry* (Van Oss, C. J., and van Regenmortel, M. H. V., Eds.) pp 201−235, Marcel Dekker, New York.
4. Ramm, K., Gehring, P., and Plückthun, A. (1999) Removal of the conserved disulphide bridges from the scFv fragment of an antibody: effect on folding kinetic and agregation. *J. Mol. Biol. 290*, 535−546.
5. Nieva, L., Honegger, A., Krebber, C., and Plückthun, A. (1997) Disrupting the hydrophobic patches at the antibody variable/constant domain interface: improved in vitro folding and physical characterization of an engineered scFv fragment. *Protein Eng. 10*, 435−444.
6. Arndt, K. M., Müller, K. M., and Plückthun, A. (1998) Factors influencing the dimer to monomer transition of an antibody single-chain Fv fragment. *Biochemistry 37*, 12918−12926.
7. Jaenicke, R. (1987) Folding and association of proteins. *Prog. Biophys. Mol. Biol. 49*, 117−237.
8. Jäger, M., and Pückthun, A. (1999a) Folding and assembly an antibody Fv fragment, a heterodimer stabilized by antigen. *J. Mol. Biol. 285*, 2005−2019.
9. Pantoliano, M. W., Bird, R. E., Johnson, S., Asel, E. D., Dodd, S. W., Wood, J. F., and Hardman K. D. (1991) Conformational stability, folding, and ligand-binding affinity of single-chain Fv

immunoglobulin fragments expressed in *Escherichia coli*. *Biochemistry 30*, 10117−10125.
10. Jäger, M., and Plückthun, A. (1999b) Domain interactions in antibody Fv and scFv fragments: effects on unfolding kinetics equilibrium. *FEBS Lett. 462*, 307−312.
11. Wörn, A., and Plückthun, A. (1998) Mutual stabilization of VL and VH in scFv antibody fragments, investigated with mutants engineered for stability. *Biochemistry 37*, 13120−13127.
12. Jäger, M., Gehring, P., and Plückthun, A. (2001) The scFv fragment of the antibody hu4D5-8: evidence for early premature domain interaction in refolding. *J. Mol. Biol. 305*, 1111−1129.
13. Gunasekaran, K., Eyles, S. J., Hagler, A. T., and Gierasch, L. M. (2001) Keeping it in the family: folding studies of related proteins. *Curr. Opin. Struct. Biol. 11*, 83−93.
14. Fontirrochi, G., Dueñas, M., Fernández de Cossío, M. E., Fuentes, P., Pérez, M., Mainet, D., Ayala, M., Gavilondo, J. V., and Duarte, C. (1993) A mouse hybridoma cell line secreting IgG and IgM antibodies specific for Hepatitis B virus surface antigen. *Biotecnol. Appl. 10*, 24−30.
15. Pentón, E., Herrera, L., Muzio, V., García, A., Duarte, C., et al. (1992) Methods for obtaining recombinant surface antigen of hepatitis B virus of higher immunogenic capacity and thereof in a vaccine preparation. European Patent Office no. EP 480−525.
16. Wörn, A., and Plückthun, A. (1999) Different equilibrium behaviour of scFv fragment: Identification, classification and improvement by protein engineering. *Biochemistry 38*, 8739−8750.
17. Pedroso, I., Agraz, A., Brito, J., Páez, R., Segredo, J. L., García, J., Pérez, M., Lugo, V., Ayala, M., Freyre, F. M., Falcón, V., Rodés, L., and Gavilondo, J. V. (1997) Single-chain Fv antibody fragment for the immunoaffinity purification of a recombinant hepatitis B virus surface antigen particle. *Minerva Biol. 9*, 68−75.
18. Ayala, M., Balint, R. F., Fernández de Cossío, M. E., Canaán Haden, L., Larrick, W. J., and Gavilondo, J. V. (1995) Variable region sequence modulates periplasmic export of a single-chain Fv antibody fragment in *Escherichia coli*. *BioTechniques, 18*, 832−842.
19. Gill, S. C., and Von Hippel, P. H. (1989) Calculation of protein extinction coefficients from amino acid sequence data. *Anal. Biochem. 182*, 312−326.
20. Uversky, V. N. (1993) Use of a fast size-chromatography to study the unfolding of protein that denatures through the molten globule. *Biochemistry 32*, 13288−13298.
21. Khurana, R., Hate, A. T., Nath, U., and Udgaonkar, J. B. (1995) pH dependence of the stability of barstar to chemical and thermal denaturation. *Protein Sci. 4*, 1133−1144.
22. Pace, C. N. (1986) Determination and analysis of urea and guanidine hydrochloride denaturation curves. *Methods Enzymol. 131*, 266−280.
23. Santoro, M. M., and Bolen, D. W. (1988) Unfolding free-energy changes determined by the linear extrapolation methods. 1. Unfolding of phenylmethanesulfonyl α-chymotrypsin using differents denaturants. *Biochemistry 27*, 8063−8068.
24. Pace, C. N. (1975) The stability of globular proteins. *Crit. Rev. Biochem. 3*, 1−43.
25. Luo, J., Iwakura, M., and Matthews, C. R. (1995) Detection of an intermediate in the thermal unfolding of a cysteine-free form of dihydrofolate from *Escherichia coli*. *Biochemistry 34*, 10669−10675.
26. Pace, C. N., Shirley, B. A., and Thomson, J. A. (1989) Measuring the conformational stability of a protein. in *Protein structure, a practical approach*, pp 311−330, IRL Press, Oxford, U.K.
27. Irún, M. P., Garcia-Mira, M. M., Sanchez-Ruiz, J. M., and Sancho, J. (2001) Native hydrogen bonds in a molten globule: the apoflavodoxin thermal intermediate. *J. Mol. Biol. 306*, 877−888.
28. Brooks, C., and Karplus, M. (1983) CHARMM: A program for macromolecular energy, minimization, and dynamics calculations. *J. Comput. Chem. 4*, 187−217.
29. Fletcher, R., and Reeves, C. M. (1977) Function minimization by conjugate gradients. *Comput. J. 7*, 149−156.
30. Edwards, E., Hubbard, E., and Brady, R. (1992) Homology modelling of antibody combining sites. *Inmunomethods 1*, 71−79.
31. Fine, R. M., Wang, H., Shenkin, P. S., Yarmush, D. L., and Levinthal, C. (1986) Predicting antibody hypervariable loop conformations. II: Minimization and molecular dynamics studies of MCPC603 from many randomly generated loop conformations. *Proteins: Struct., Funct., Genet. 1*, 342−362.
32. Jones, T. A., and Thirup, S. (1986) Using known substructures in protein model building and crystallography. *EMBO J. 5*, 819−822.
33. Shenkin, P. S., Yarmush, D. L., Fine, R. M., Wang, H. J., and Levinthal C. (1987) Predicting antibody hypervariable loop conformation. I. Ensembles of random conformations for ringlike structures. *Biopolymers 26*, 2053−2085.
34. Martin, A. C., Cheetham, J. C., and Rees, A. R. (1991) Molecular modelling of antibody combining sites. *Methods Enzymol. 203*, 121−153.
35. Kieber-Emmons, T., Lin, C., Foster, M. H., and Kleyman, T. R. (1999) Antiidiotypic antibody recognizes an amiloride binding domain within the alpha subunit of the epithelial Na^+ channel. *J. Biol. Chem. 274*, 9648−9655.
36. Satow, Y., Cohen, G. H., Padlan, E. A., and Davies, D. R. (1986) Phosphocholine binding immunoglobulin Fab McPC603. An X-ray diffraction study at 2.7 Å. *J. Mol. Biol. 190*, 593−604.
37. Connolly, M. L. (1983) Solvent-accessible surfaces of proteins and nucleic acids. *Science 221*, 709−713.
38. Vuilleumier, S., Sancho, J., Loewenthal, R., and Fersht, A. R. (1993) Circular dichroism studies of barnase and its mutants: characterization of the contribution of aromatic side chains. *Biochemistry 32*, 10303−10313.
39. Schmid, F. X. (1989) Spectral methods of characterizing protein conformational changes. in *Protein Structure, a practical approach*, IRL Press, Oxford, U.K.
40. Wong, K. P., and Tanford, C. (1973) Denaturation of bovine carbonic anhydrase B by guanidine hydrochloride. A process involving separable sequential conformational transitions. *J. Biol. Chem. 248*, 8518−8523.
41. Kuwajima, K., Nitta, K., Yoneyama, M., and Sugai, S. (1976) Three-state denaturation of α-lactalbumin by guanidine hydrochloride. *J. Mol. Biol. 106*, 359−373.
42. Luo, Y., Kay, M. S., and Baldwin, R. L. (1997) Cooperativity of folding of the apomyoglobin pH 4 intermediate studied by glycine and proline mutations. *Nat. Struct. Biol. 4*, 925−930.
43. Sanchez-Ruiz, J. M., Lopez-Lacomba, J. L., Cortijo, M., and Mateo, P. L. (1988) Differential scanning calorimetry of the irreversible thermal denaturation of thermolysin. *Biochemistry 27*, 1648−1652.
44. Myers, J. K., Pace, C. N., and Scholtz, J. M. (1995) Denaturant *m* values and heat capacity changes: relation to changes in accessible surface areas of protein unfolding. *Protein Sci. 4*, 2138−2148.
45. Genzor, C. G., Beldarraín, A., Gómez-Moreno, C., López-Lacomba, J. L., Cortijo, M., and Sancho, J. (1996) Conformational stability of apoflavodoxin. *Protein Sci. 5*, 1376−1388.
46. Eigenbrot, C., Randal, M., Presta, L., Carter, P., and Kossiakoff, A. A. (1993) X-ray structures of the antigen-binding domains from three variants of humanised anti-p185HER2 antibody 4D5 and comparison with molecular modelling. *J. Mol. Biol. 229*, 969−995.
47. Martsev, S. P., Chumanevich, A. A., Vlasov, A. P., Dubnovitsky, A. P., Tsybovsky, Y. I., Deyev, S. M., Cozzi, A., Arosio, P., and Kravnuck, Z. I. (2000) *Biochemistry*, *39*, 8047−8057.
48. Fersht, A. R., Matouschek, A., and Serrano, L. (1992) The folding of an enzyme. I. Theory of protein engineering analysis of stability and pathway of protein folding. *J. Mol. Biol. 224*, 771−782.
49. Jamin, M., and Baldwin, R. L. (1996) Refolding and unfolding kinetics of the equilibrium folding intermediate of apomyoglobin. *Nat. Struct. Biol. 3*, 613−618.
50. Kay, M. S., and Baldwin, R. L. (1996) Packing interactions in the apomyoglobin folding intermediate. *Nat. Struct. Biol. 3*, 429−445.
51. Sancho, J., Bueno, M., Campos, L. A., Fernández-Recio, J., Irún, M. P., López, J., Machicado, C., Pedroso, I., and Toja, M. (2002) The 'relevant' stability of proteins with equilibrium intermediates. *Sci. World 2*, 1209−1215.
52. Gulliver, G. A., Rumbley, C. A., Carrero, J., and Voss, E. W., Jr. (1995) Relative conformational stabilities of single-chain pocket and groove-shaped antibody active sites including HCDR transplant intermediates. *Biochemistry 34*, 5158−5163.
53. Tan, P. H., Sandmaier, B. M., and Stayton, P. S. (1998) Contributions of a highly conserved V_H/V_L hydrogen bonding interaction to scFv folding stability and refolding efficiency. *Biophys. J. 75*, 1473−1482.
54. Jung, S., Honegger, A., and Plückthun, A. (1999) Selection for improved protein stability by phage display. *J. Mol. Biol. 294*, 163−180.
55. Wörn, A., and Plückthun, A. (2001) Stability engineering of antibody single-chain Fv fragments. *J. Mol. Biol. 305*, 989−1010.

BI025742E